Temperature-independent refractive index measurement based on Fabry–Perot fiber tip sensor modulated by Fresnel reflection

Yue Ma (马 玥)[1*], Xueguang Qiao (乔学光)[1], Tuan Guo (郭 团)[2], Ruohui Wang (王若晖)[1], Jing Zhang (张 菁)[1], Yinyan Weng (翁银燕)[1], Qiangzhou Rong (荣强周)[1], Manli Hu (忽满利)[1], and Zhongyao Feng (冯忠耀)[1]

[1]*Department of Physics, Northwest University, Xi'an 710069, China*

[2]*Institute of Photonics Technology, Jinan University, Guangzhou 510632, China*

[*]*Corresponding author: yuemanwu@gmail.com*

Received October 11, 2011; accepted December 12, 2011; posted online March 6, 2012

A simple fiber tip sensor for refractive index (RI) measurement based on Fabry–Perot (FP) interference modulated by Fresnel reflection is proposed and demonstrated. The sensor head consists of an etching-induced micro air gap near the tip of a single-mode fiber. The microgap and the fiber tip function as two reflectors to form a FP cavity. The external RI can be unambiguously measured by monitoring the fringe contrast of the interference pattern from the reflection spectrum. The experimental results show that the proposed sensor achieves temperature-independent RI measurement with good linear response. The proposed sensor achieves a high RI resolution of up to 3.4×10^{-5} and has advantages of low cost and easy fabrication.

OCIS codes: 060.2370, 120.2230.
doi: 10.3788/COL201210.050603.

High-quality refractive index (RI) sensing is very important in biological and chemical applications, which are always operated in the presence of other environmental perturbations (particularly temperature). One attractive scheme is based on fiber-optic Fabry–Perot (FP) (FFP) interferometers, which have advantages of compact size, linear response, high sensitivity, and low temperature dependence[1−8]. However, conventional FFP RI sensors usually work based on phase modulation interferences in response to changes in the RI of the medium filling the cavity[1−3]. As a result, their reliabilities are deteriorated by the contaminants deposited on the FP cavity during the cavity-filling process. Recently, a filling-free FP fiber tip sensor, which had a hybrid structure made by laser micromachining a sealed FP air cavity near a single-mode fiber (SMF) tip, was proposed[4]. The air cavity was not a sensing element but served as an in-fiber reflector. The light reflected from the air cavity interfered with that reflected from the fiber tip to form another fiber FP cavity. The variation in the surrounding RI changed the Fresnel reflection (FR) at the fiber tip, and the RI was determined by measuring the fringe contrast (FC) of the interference spectrum. A similar structure was also demonstrated by inserting a hollow-core fiber (HOF) between a SMF and a downstream multimode fiber (MMF)[5]. The inserted HOF formed an air cavity and functioned as a reflector. Similarly, the RI variation was measured when the FC varied because of the changed FR at the MMF tip. These devices avoid undesirable cavity-filling processes and allow the measurement of the RI of a liquid at the fiber tip using the FP interference modulated by FR, which has also been widely used in other works[6−9]. Moreover, these devices provide high accuracy and reliability, but their fabrication is expensive and complex due to the requirement of a laser micromachining technique[4] or the special HOF[5].

In contrast, wet chemical etching is a simple and cost-effective method for fabricating FFP interferometers, and devices fabricated using this method have been proven to be excellent sensors in, e.g., pressure, strain, temperature, and thin-film measurements[10−14]. This technique uses different etching rates between the Ge-doped silica fiber core and the pure silica cladding and thus results in a small pit on the fiber end face. A FFP interferometer can be obtained[15] by simply splicing the etched fiber to another fiber.

This letter incorporates the FR modulation mechanism into an etching-assisted FFP interferometer and demonstrates a cost-effective FP fiber tip sensor for high-quality RI measurement. The sensor head consists of an etching-induced micro air gap near a SMF tip, and the microgap and fiber tip function as two reflectors to form a FP cavity. Temperature-independent RI measurement was experimentally achieved with good linearity and high sensitivity by measuring the FC of the interference spectrum reflected from the sensor head. Furthermore, the sensor showed a potential for simultaneous RI and temperature measurement by simultaneously tracking the wavelength shift of the interference pattern. Such a sensor not only has advantages similar to those of previous FFP RI devices made by other expensive techniques but also offers easy and low-cost fabrication, which makes it a good candidate for practical sensing applications.

The FP fiber tip sensor was fabricated through cleaving, chemical etching, and fusion splicing. A conventional SMF was first cleaved and etched with hydrofluoric acid (40% per weight). The etching rate of the fiber core was faster than that of the cladding. Thus, a small pit, with a diameter and depth of approximately 27 and 5 μm, respectively, was formed on the fiber end face, as shown in

Fig. 1(a). Then, the etched fiber was spliced to another SMF. The splicing point hence contained a micro air gap that served as the first reflector of the FP cavity. A shorter arc time and lower arc power were preferred during the splicing process to avoid overmelting and hence guarantee the existence of the air gap. Moreover, a small gap width was required as the air gap caused additional transmission loss due to beam divergence. This small gap width can be achieved by properly controlling the etching time and splicing conditions. The experimental results show that the optimum etching time is 4 min and the arc time and power are 400 ms and 100 units, respectively (using the Fujikura FSM-60S fusion splicer). The achieved microgap was thin enough (∼3 μm) to perform as a single reflector. Finally, the other side of the spliced fiber was cleaved near the splice to produce the second reflector. The fabricated device is shown in Fig. 1(b). The cavity length was determined by the distance between the air gap and the fiber tip, which was estimated to be 597.96 μm. Then, a broadband source was used to illuminate the fabricated device through an optical circulator. The reflection spectrum was recorded using an optical spectrum analyzer (OSA), and the results are shown in Fig. 2. A clear interference pattern was observed with a FC of 12 dB, which was sufficient for most applications and could be further improved by employing a fiber with a higher core RI and by optimizing etching and splicing conditions. The air gap probably caused a slowly varying envelope of the spectrum. However, it was not observed in the experiment for the measurement range of 1 584–1 594 nm because of the very large free spectral range (FSR) induced by the quite small air-gap width. Therefore, the modulation on the interference pattern formed by the fiber cavity, which was induced by the slowly varying envelope from the air-gap cavity, was very minimal, and its effect on the experimental results could be neglected.

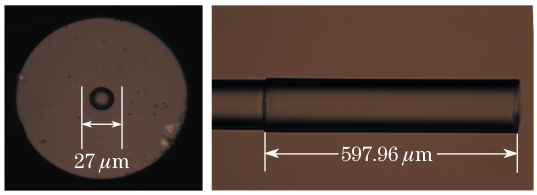

Fig. 1. Photograph of (a) the end face of the etched fiber and (b) the fabricated FP fiber tip sensor.

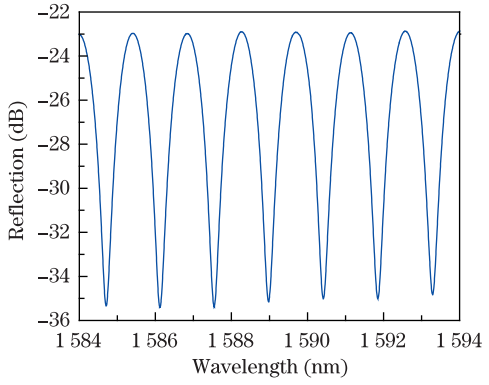

Fig. 2. Reflection spectrum of the fabricated sensor (with a clear FC of 12 dB).

A theoretical model of the two-beam interferometer was established to explain the principle of the proposed RI sensor. The fiber tip is supposed to be dipped into the liquid whose RI is to be measured. Considering that the reflections on both reflectors belong to the FR, their reflectivity values R_1 and R_2 can be calculated using the well-know Fresnel equation:

$$R_1 = \left|\frac{n_0 - 1}{n_0 + 1}\right|^2, \quad R_2 = \left|\frac{n_0 - n_l}{n_0 + n_l}\right|^2, \tag{1}$$

where n_0 (1.467 for the SMF used at a 1 550 nm WL) and n_l are the RIs of the fiber core and liquid, respectively. The total contribution from the multipath reflections is less than 0.1% because of the low reflectivity values (on the order of a few percentages) and can therefore be neglected[4]. In this case, the low-finesse FP sensor can be approximated as a two-beam interferometer, as shown in Fig. 3, where A_1 and A_2 are the transmission loss factors of the two reflectors, respectively. The total reflected field E_r can be described as

$$E_r = E_i[\sqrt{R_1} + (1 - R_1)(1 - A_1)\sqrt{R_2}e^{-j2\beta L}], \tag{2}$$

where E_i is the input field, β is the propagation constant of the guided mode of the fiber, and L is the cavity length. Here, the propagation loss of the fiber cavity is neglected for simplicity. Thus, the normalized reflection spectrum can be obtained as

$$I(\lambda) = \left|\frac{E_r}{E_i}\right|^2 = R_1 + (1 - A_1)^2(1 - R_1)^2 R_2 + 2\sqrt{R_1 R_2}(1 - A_1)(1 - R_1)\cos\left(\frac{4\pi n_o L}{\lambda}\right), \tag{3}$$

where λ is the optical wavelength in the vacuum. As the relative phase difference ($\varphi = \frac{4\pi n_o L}{\lambda}$) of the two interfering beams becomes an even or an odd number of π, the reflected signal alternately reaches its maximum $I_{max}(\lambda)$ and minimum $I_{min}(\lambda)$. An interference pattern hence appears in the reflection spectrum. The FC of the interference pattern is given by

$$\begin{aligned} C &= 10\lg_{10}\left[\frac{I_{max}(\lambda)}{I_{min}(\lambda)}\right] \\ &= 20\lg_{10}\left[\frac{\sqrt{R_1} + (1 - R_1)(1 - A_1)\sqrt{R_2}}{\sqrt{R_1} - (1 - R_1)(1 - A_1)\sqrt{R_2}}\right] \\ &= 20\lg_{10}\left[\frac{\sqrt{R_1} + (1 - R_1)(1 - A_1)(n_0 - n_l)/(n_0 + n_l)}{\sqrt{R_1} - (1 - R_1)(1 - A_1)(n_0 - n_l)/(n_0 + n_l)}\right]. \end{aligned} \tag{4}$$

When the liquid RI (n_l) changes, the reflectivity (R_2) at the fiber tip is changed, and subsequently, the FC varies. Moreover, the thermo-optic coefficient of the fiber is very small and the temperature variation has negligible effect on n_0, R_1, and A_1 in Eq. (4). Thus, the RI can be determined independent of temperature by measuring the FC of the interference spectrum.

Meanwhile, considering that the phase difference of the two adjacent spectral minima is 2π, the cavity length can be expressed as

$$L = \frac{\lambda_1 \lambda_2}{2n_0(\lambda_2 - \lambda_1)}. \tag{5}$$

As shown, an inverse relationship between the cavity length and the FSR exists, indicating that the interference spectrum can be tailored simply by controlling the cavity length by properly performing the cleaving process during sensor fabrication. According to the measured spectrum in Fig. 2, the cavity length of the fabricated device is calculated as 598.14 μm (λ_1=1 588.974 nm, λ_2=1 590.416 nm), which is very close to that observed under a microscope (597.96 μm).

The performance of the fabricated RI sensor was experimentally characterized, as shown in Fig. 4. A series of glycerin solutions with different volume concentrations was prepared as samples, and the corresponding RIs calibrated by an Abbe refractometer ranged from 1.3333 to 1.4069. The sensor head is dipped into each solution to get the corresponding reflection spectrum, and its spectral response to the change in RI is shown in the inset of Fig. 5. As shown, the FC decreases monotonically with increasing RI, as expected, whereas the wavelength mainly remains unchanged. The decrease in FC was caused by the reduced FR at the fiber tip exposed to RI samples. The RI sensitivity was determined by using a dip at a wavelength of approximately 1 591.9 nm and an adjacent peak at 1 592.6 nm and by calculating the corresponding FC for each RI measurement. Figure 5 shows the FC as a function of RI. The linear fitting shows an overall sensitivity of 29.7 dB/RIU (RI unit) within the sensing range from 1.3333 to 1.4069, which is usually relevant for biological and chemical applications. This high sensitivity is a result of the micromachining-based interference sensing technique. Given that the amplitude resolution of the OSA is 0.001 dB, the RI resolution is estimated to be 3.4×10^{-5}, which is comparable to those of existing FP sensors with FRs. However, the fabrication process of the proposed device is much easier and cost effective, as shown in Table 1.

The temperature effect was studied by fixing the sensor on a heating board and cycling the temperature in a range of 30–120 °C. The spectral response for the heating

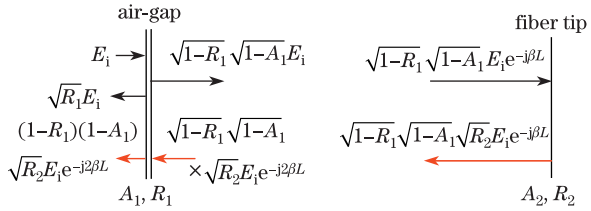

Fig. 3. Theoretical model of the FP fiber tip RI sensor.

Table 1. Comparison of the Existing FP-based RI Sensors with FRs and the Proposed Sensor

First Reflector	Fabrication Technique	RI Resolution
Air Gap[4]	Laser Micromachining	3.7×10^{-5}
HOF[5]	Fiber Drawing Technique	6.2×10^{-5}
FBG[6]	UV Beam-Scanning Phase-Mask Technique	$\sim 10^{-3}$
Air Gap (the Proposed Sensor)	Wet Chemical Etching	3.4×10^{-5}

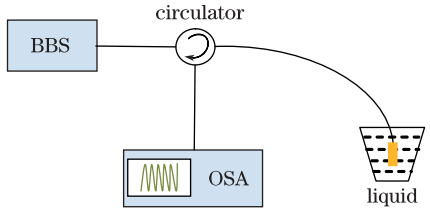

Fig. 4. Schematic diagram of the experimental setup for RI measurement.

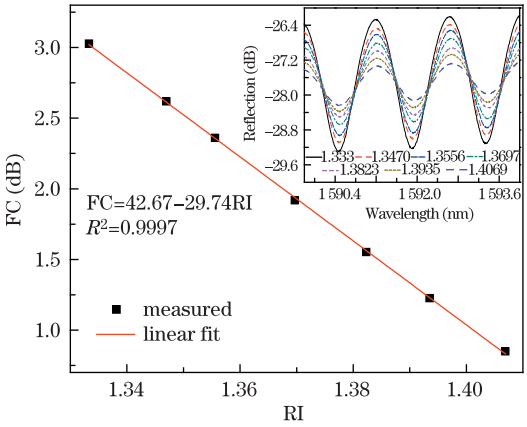

Fig. 5. FC as a function of RI. The inset shows the spectral response to the RI change.

process is illustrated in the inset of Fig. 6. As shown, the interference pattern horizontally shifts toward a longer wavelength with increasing temperature, whereas the observed amplitude variation is minimal. The dip at a wavelength of approximately 1 584.7 nm (at 30 °C) and the adjacent peak at 1 585.4 nm were selected for the temperature characterization of the sensor. Figure 6 shows the variations of the FC due to temperature changes. The observed FC variations are less than 1%, indicating the sensor's ability to perform temperature-independent RI measurement. Figure 7 shows the dip wavelength as a function of temperature. Linear responses are obtained in both heating and cooling processes with a sensitivity of 11.1 pm/°C, indicating that, by simultaneously tracking the dip wavelength, the sensor has the potential to measure temperature simultaneously in the RI sensing region. This simultaneous measurement is essentially important for liquid RI sensing in biological and chemical applications, where the detected RIs of most liquids are temperature dependent (i.e., thermally induced RI variation). Thus, real-time temperature information is necessary to calibrate the detected data and to achieve high-quality RI measurement. Details of this endeavor need further experimental studies and are beyond the scope of the current paper.

In conclusion, a simple RI sensor based on a compact FP fiber tip structure fabricated via chemical etching and splicing is demonstrated. The RI variation due to the FC variation, which is, in turn, due to the changed FR at the SMF tip, is measured. The experimental results show that such an interference-based sensor can achieve temperature-independent RI measurement with good linearity and high sensitivity over a biologically desirable sensing range. In addition, the sensor has shown

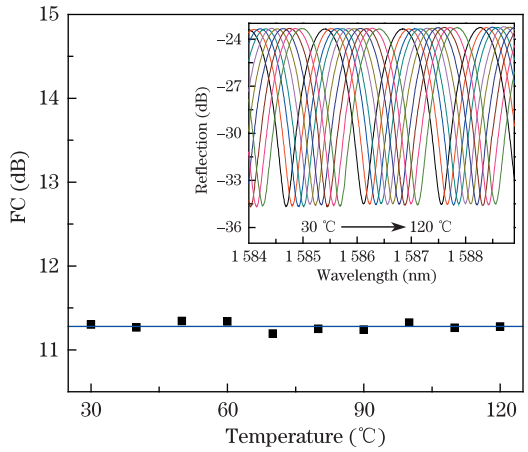

Fig. 6. FC measured at different temperatures. The inset shows the spectral response to the temperature change.

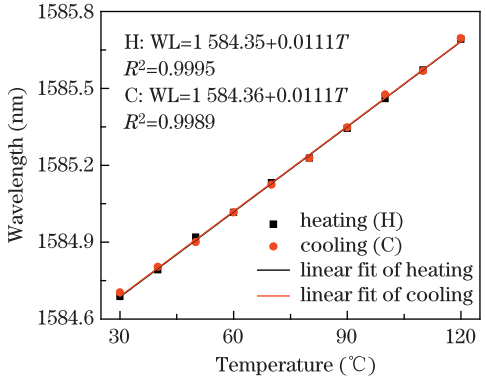

Fig. 7. Dip WL as a function of temperature. WL: wavelength.

its potential for simultaneous RI and temperature measurement. Compared with the RI sensors based on similar structures fabricated using other expensive techniques, the proposed device possesses a comparable resolution but offers advantages of easier fabrication and lower cost. These advantages make the sensor a promising candidate in practical sensing applications, such as biological molecule binding monitoring, chemical liquid concentration detection, etc.

This work was supported by the National Natural Science Foundation of China (Nos. 60727004 and 61077060), the National "863" Program of China (Nos. 2007AA03Z413 and 2009AA06Z203), the Ministry of Education Project of Science and Technology Innovation (No. Z08119), the Ministry of Science and Technology Project of International Cooperation (No. 2008CR1063), the Shaanxi Province Project of Science and Technology Innovation (Nos. 2009ZKC01-19 and 2008ZDGC-14), the Guangdong Nature Science Foundation (No. S2011010001631), and the Fundamental Research Funds for the Central Universities of China (No. 11611601).

References

1. G. Z. Xiao, A. Adnet, Z. Zhang, F. G. Sun, and C. P. Grover, Sensor Actuator A Phys. **118,** 177 (2005).
2. T. Wei, Y. Han, Y. Li, H. Tsai, and H. Xiao, Opt. Express **16,** 5764 (2008).
3. Y. Tian, W. Wang, N. Wu, X. Zou, C. Guthy, and X. Wang, Sensors **11,** 1078 (2011).
4. Z. L. Ran, Y. J. Rao, W. J. Liu, X. Liao, and K. S. Chiang, Opt. Express **16,** 2252 (2008).
5. H. Y. Choi, G. Mudhana, K. S. Park, U. Paek, and B. H. Lee, Opt. Express **18,** 141 (2010).
6. S. F. O. Silva, P. Caldas, J. L. Santos, and F. M. Araujo, Opt. Eng. **47,** 054403 (2008).
7. Y. Gong, Y. Guo, Y. J. Rao, T. Zhao, and Y. Wu, IEEE Photon. Technol. Lett. **22,** 1708 (2010).
8. M. S. Ferreira, L. Coelho, K. Schuster, J. Kobelke, J. L. Santos, and O. Frazao, Opt. Lett. **36,** 4029 (2011).
9. S. Silva, O. Frazao, J. L. Santos, and F. X. Malcata, Sensor Actuator B Chem. **161,** 88 (2012).
10. Y. Z. Zhu, K. L. Cooper, G. R. Pickrell, and A. Wang, J. Lightwave Technol. **24,** 861 (2006).
11. E. Cibula and D. Donlagic, Opt. Express **15,** 8719 (2007).
12. T. Zhao, Y. Gong, Y. Rao, Y. Wu, Z. Ran, and H. Wu, Chin. Opt. Lett. **9,** 050602 (2011).
13. P. A. R. Tafulo, P. A. S. Jorge, J. Santos, F. M. Araujo, and O. Frazao, IEEE Sens. J. **12,** 8 (2011).
14. Y. Zhang, X. P. Chen, Y. X. Wang, K. L. Cooper, and A. Wang, J. Lightwave Technol. **25,** 1797 (2007).
15. V. R. Machavaram, R. A. Badcock, and G. F. Fernando, Sensor Actuator A Phys. **138,** 248 (2007).